Supporting Information

Nanosilica polyamidoamine dendrimers for Enhanced Direct Air CO_2 Capture

Vaishnavi Kulkarni, Jayashree Parthiban, and Sanjay Kumar Singh*

Department of Chemistry, Indian Institute of Technology Indore, Simrol, Indore 453552, Madhya Pradesh, India

email: sksingh@iiti.ac.in

……

Table of Contents

1. Experimental section

1.1 Materials. Tetraethyl orthosilicate (TEOS), (3-Aminopropyl) triethoxysilane (APS), methyl acrylate (MA) and ethylene diamine (EDA) and were procured from Sigma-Aldrich. Anhydrous ethanol was purchased from Changshu Hongsheng Fine Chemical Company (99.9%), aqueous ammonia from Rankem, and HPLC methanol from Merck. All chemicals were used as received without any further purification. The high purity N_2 (99.99%) and 400 ppm CO_2 in He (99.99%; < 0.0002% H_2O) were supplied by Inox air products Pvt. Ltd. and Sigma gases and services, India, respectively.

1.2. Synthesis of nanosilica. To prepare Nanosilica (NS), initially, 16 mL of tetraethyl orthosilicate (TEOS) was added to 200 mL of ethanol in the presence of 16 mL of ammonia solution and placed in a water bath under ultrasonic vibration for 2 hours.[1] The resulting white solid contents were then centrifuged and washed with water and ethanol until the pH of the supernatant is neutral. The white solid part was then dried at 80 °C under vacuum for 12 hours.

1.3. Synthesis of one-pot aminosilane modified nanosilica. The standard process for preparing one-pot aminosilane modified nanosilica (NS-G0) involves the addition of 16 mL of tetraethyl orthosilicate (TEOS) to a mixture containing 16 mL of aqueous ammonia, and 200 mL of ethanol.[2] The resulting mixture is placed in water bath under ultrasonication for 2 hours to obtain a solid white precipitate. The solid white precipitate was washed with distilled water and ethanol several times until neutral pH was attained. The precipitate is then dried in a vacuum oven at 70 °C for 12 hours.

1.4 Synthesis of polyamidoamine nanosilica dendrimers. The process of grafting and propagating hyperbranched polyamidoamine nanosilica surface was attained through a two-step procedure: (1) initiating a Michael addition reaction between methyl acrylate (MA) and the amino groups present on the surface, followed by (2) the amidation of resultant terminal ester groups using ethylenediamine (EDA).[3] The Michael addition of methyl acrylate (MA) to the amino groups on the surface was performed by the addition of 0.42 g of NS-G0 to 7 mL of methanol containing 0.84 g of MA, in a round-bottom flask. Subsequently, the mixture was stirred at 50°C for 24 hours. The resulting white powder (NS-G0.5) was isolated by multiple washes with methanol (or washed with methanol thrice), and subsequently dried at room temperature. The amidation of terminal ester groups was achieved by the addition of 0.84 g of EDA to 7 mL methanol containing G0.5 white powder and heated at 50 °C for 24 hours.

Subsequently, the resulting white powder (NS-G1.0) was washed with methanol several times and dried under vacuum at room temperature. Further the hyperbranched polymer was synthesized by repeating the steps involving Micheal addition with MA and amidation with EDA till the hyperbranched polyamidoamine NS-G4.0 dendrimers were obtained.

2. Characterization. Prior to the analysis of textural properties, pristine NS and PAMAM modified NS adsorbents are outgassed at 110 °C for 3 hours under ultrahigh vacuum, respectively. The low temperature (110 °C) outgassing condition is chosen to avoid the amine loss.[4,5] Powder X-ray diffraction (P-XRD) data is recorded on a Rigaku SmartLab advanced diffractometer with monochromatic Cu Kα radiation (λ = 0.154 nm) at a step size of 0.02° and counting time of 3s/step over a 2θ range from 5 to 45°. The morphology and microstructure of adsorbents are observed under field emission scanning electron microscopy (FESEM) (Carl ZEISS Supra-55, accelerating voltage of 5 kV) and transmission electron microscopy (TEM) (FEI Tecnai G2, F30, operating voltage 300 kV). EDS and elemental mapping analysis are performed on EDAX Octane ELITE T70 (operating voltage 300 kV). The N_2 physisorption measurements are carried out at −196 °C using a Quantachrome Autosorb iQ_2 TPX automated gas sorption system to investigate the physicochemical properties (surface area and pore volume) of the adsorbents. The specific surface area of adsorbents is calculated using the Brunauer-Emmett-Teller (BET) equation in the relative pressure (P/P_0) range of 0.05-0.30 from the adsorption branch. Pore size distribution is calculated using the NLDFT (Non-Local Density Functional Theory) model.[6] The total pore volume is calculated based on the total amount of adsorbed N_2 at P/P_0 of 0.99. The amine loading of the adsorbent is determined by using a Mettler-Toledo TGA/DSC-1 thermal analyzer. The data is recorded by heating the sample under nitrogen flow from 25 to 800 °C with a ramp rate of 5 °C/min. Amine loading is defined as the mass percentage of the amine loss to the total sorbent mass during the temperature range of 120–800 °C. The molecular composition of the adsorbent is identified by Fourier transform infrared (FT-IR, PerkinElmer) spectrometry in attenuated total reflection (ATR) mode in the wavenumber range 4000−400 cm^{-1}.

3. Evaluation of CO_2 adsorption performance

3.1 CO_2 uptake under direct air capture condition (400 ppm CO_2 in He). To assess the efficacy of NS-PAMAM dendrimers, for carbon dioxide (CO_2) adsorption during a simulated Temperature Swing Adsorption (TSA) cycle,[7] we performed thermogravimetric measurements using a Mettler Toledo TGA/DSC-1 instrument. The TSA cycle involved four distinct steps:

desorption, cool down, adsorption, and heat up. In the experimental procedure, a 0.012 g powder sample was placed in an alumina crucible and subjected to a 3-hour outgassing period at 110 °C under a nitrogen flow of 20 mL/min to eliminate moisture (step I). Subsequently, the temperature of the adsorbent was reduced to 30 °C over 27 minutes (step II) and stabilized for 10 minutes under a nitrogen flow (step III). Following this, the adsorbent was exposed to a mixture of 400 ppm CO_2 in helium (20 mL/min) for 12 hours at 30 °C (step IV). The adsorption duration was carefully selected to ensure the attainment of pseudo-equilibrium adsorption capacity, with the weight change remaining below 8×10^{-3} % per min.[8]

3.2 Direct CO_2 adsorption under indoor air condition. In this investigation, the synthesized PAMAM dendrimers were assessed for their ability to capture CO_2 from indoor air using a flow-through setup. Each sample, weighing 0.1 g, was placed within an adsorbent bed fitted with a heating tape. During the 0.5-hour adsorption phase, an airflow of approximately 2 L/min was directed through the adsorbent bed. For desorption, the adsorbent bed was heated to 80 °C while for 0.5 h. The concentration of CO_2 in the chamber was continuously monitored using a CO_2 analyzer (ATS-206A), and the adsorption capacity was determined by integrating the quantity of CO_2 captured over the 0.5 h period.

3.3 Reutilizing CO_2 Released from NS-G3.0 during desorption by conversion to formate. Further, to reutilize the CO_2 produced during the desorption of CO_2 captured over NS-G3.0, we adopted a two-step CO_2 hydrogenation process. NS-G3.0 (0.1 g) underwent an adsorption cycle at 30 °C and 400 ppm CO_2 and later for the desorption step heated at 80 °C for 0.5 h. The released gas CO_2 (confirmed by GC-TCD analysis) is passed through KOH (1 mmol) in water (5 mL) for 2 h to capture CO_2 (as CO_3^{2-}, confirmed by ^{13}C NMR spectra). The effluent gas was analyzed to have only N_2 gas (as confirmed by GC-TCD), confirming the complete capture of CO_2 released during the desorption process. Later, this solution containing CO_3^{2-} is transferred to a 50 mL high-pressure reactor and pressurized with H_2 gas (20 bar) and **[Ru]-1** (0.025 mmol) heated at 80 °C for 6 h. After cooling to room temperature, the gas is released, and the resulting solution is finally analyzed by ^1H NMR (D_2O) from the reactor.

3.4 Reutilizing CO_2 Released from NS-G3.0 during desorption by conversion to $CaCO_3$ pellets. The experimental setup involved utilizing desorbed CO_2 obtained from NS-G3.0. The desorbed CO_2 was passed through a 5 mL solution of $Ca(OH)_2$.[10] The desorption process was carried out under N_2, at 80°C for 0.5 h. Subsequently, the desorbed CO_2 was bubbled through the $Ca(OH)_2$ solution until the lime water exhibited a milky appearance, indicating the

formation of a white precipitate. The formed precipitate, identified as $CaCO_3$, was carefully separated, washed thoroughly, and subjected to centrifugation. Afterward, the precipitate was dried and then transformed into small pellets, making it ready for further applications in line with the objective of repurposing desorbed CO_2 from NS-G3.0 into a useful product.

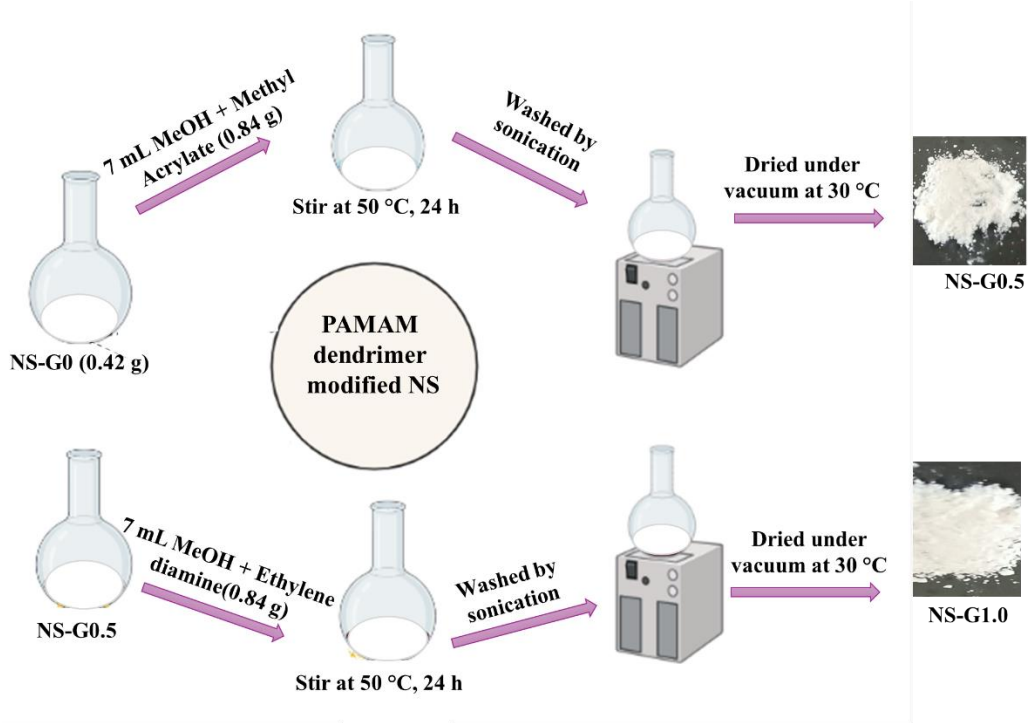

Scheme S1. Preparation of NS-PAMAM dendrimers.

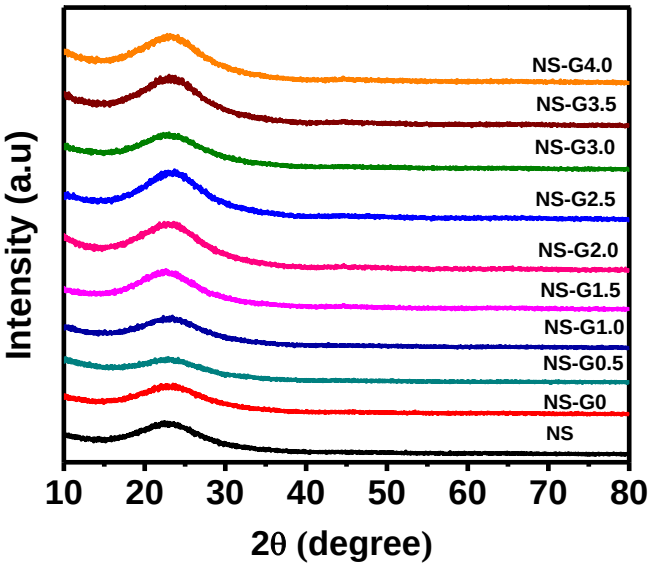

Figure S1. P-XRD patterns of NS-PAMAM dendrimers.

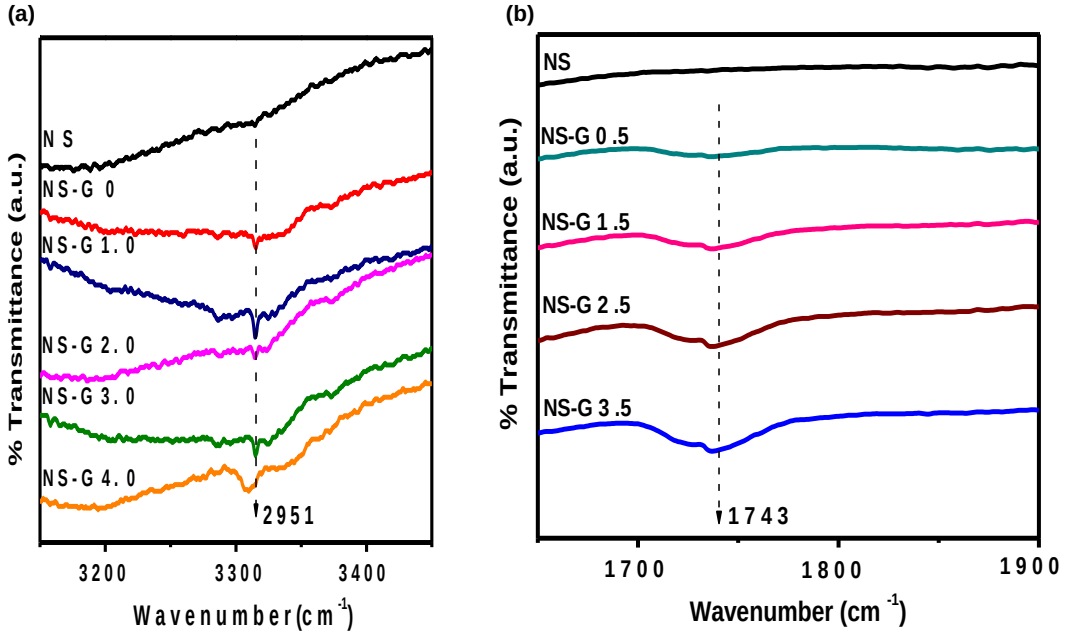

Figure S2. FTIR spectra of (a) NS, NS-G0, NS-G1.0, NS-G2.0, NS-G3.0, and NS-G4.0 and (b) NS, NS-G0.5, NS-G1.5, NS-G2.5, and NS-G3.5.

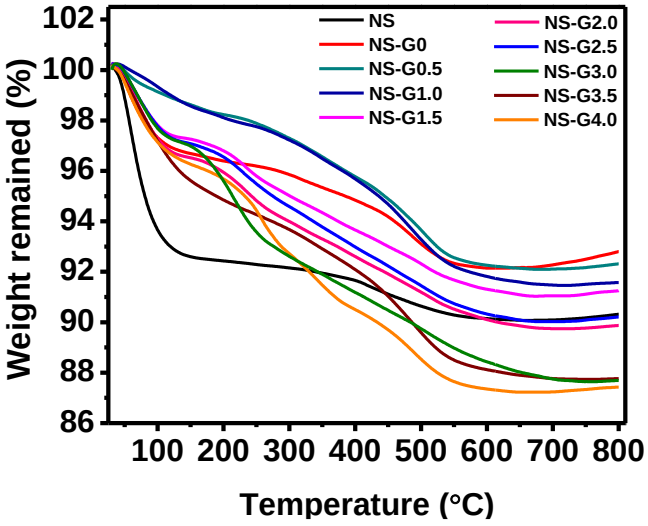

Figure S3. TGA curves of NS-PAMAM dendrimers.

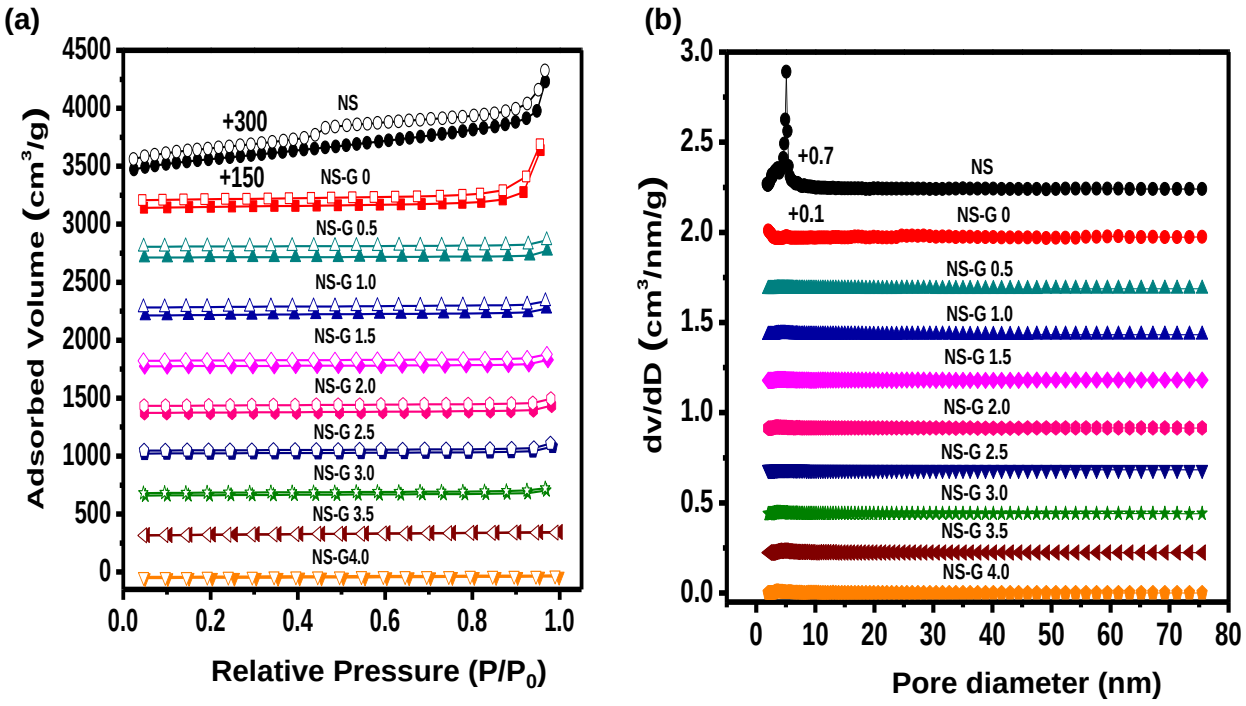

Figure S4. (a) N_2 adsorption-desorption isotherm at -196 °C and (b) corresponding pore size distribution obtained using NLDFT method of NS-PAMAM dendrimers.

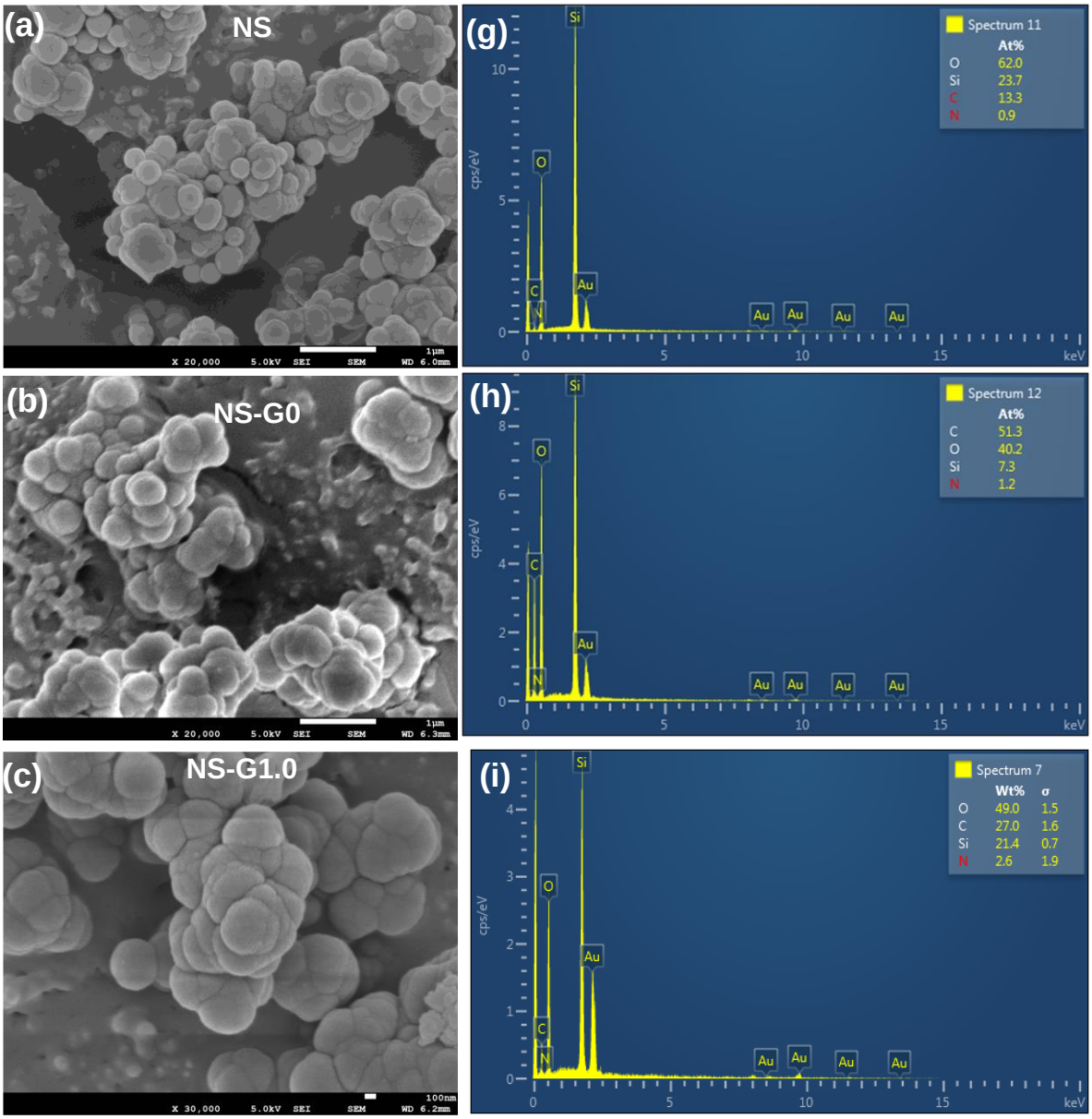
(a)
NS
X 20,000 5.0kV SEI SEM WD 6.0mm
1μm
(b)
NS-G0
X 20,000 5.0kV SEI SEM WD 6.3mm
1μm
(c)
NS-G1.0
X 30,000 5.0kV SEI SEM WD 6.2mm
100nm
(g)
Spectrum 11
At%
O 62.0
Si 23.7
C 13.3
N 0.9
(h)
Spectrum 12
At%
C 51.3
O 40.2
Si 7.3
N 1.2
(i)
Spectrum 7
Wt% σ
O 49.0 1.5
C 27.0 1.6
Si 21.4 0.7
N 2.6 1.9
cps/eV
keV
Si
O
C
N
Au

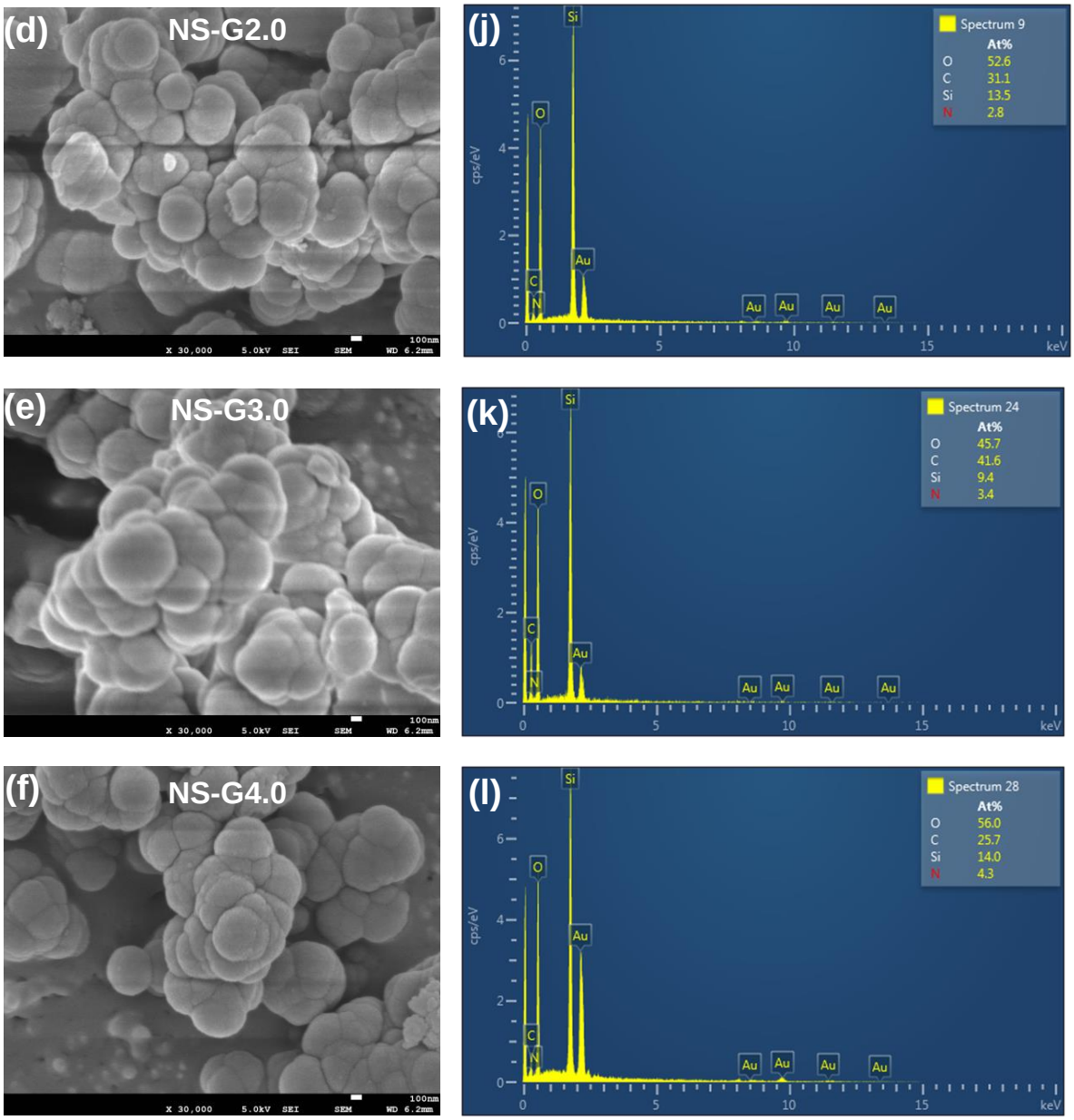

Figure S5. (a-f) FESEM images of (a) NS, (b) NS-G0, (c) NS-G1.0, (d) NS-G2.0, (e) NS-G3.0, (f) NS-G4.0 and (g-l) and their corresponding EDS spectra.

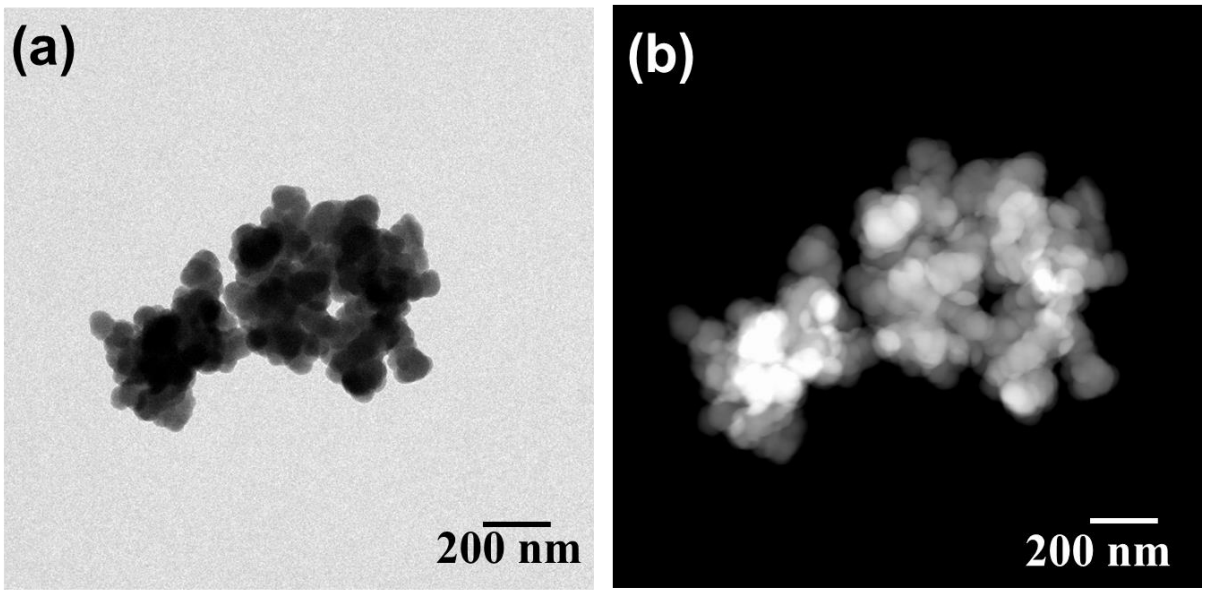

Figure S6. (a) TEM and (b) HAADF-STEM images of NS-G0.

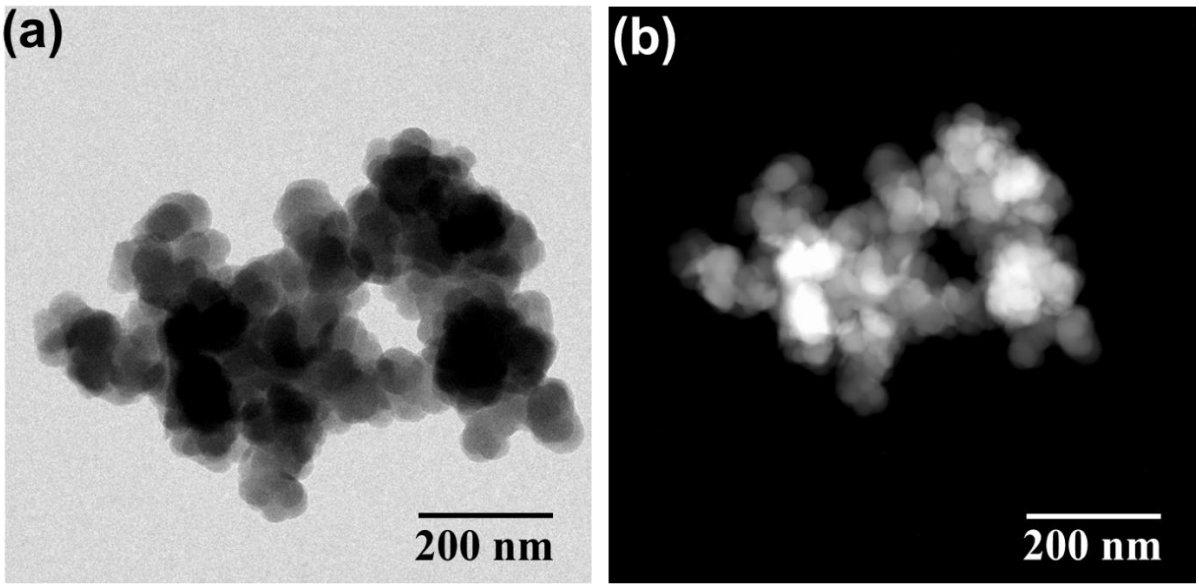

Figure S7. (a) TEM and (b) HAADF-STEM images of NS-G3.0.

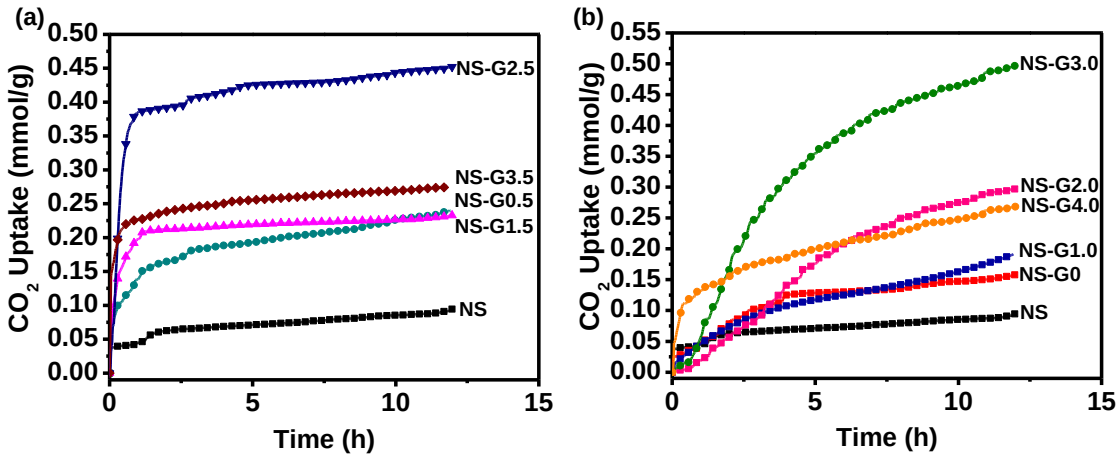

Figure S8. CO_2 uptake (400 ppm CO_2 in helium), 30 °C of (a) NS, NS-G0.5, NS-1.5, NS-G2.5, and NS-G3.5 and (b) NS-G0, NS-G1.0, NS-G2.0, NS-3.0, and NS-G4.0.

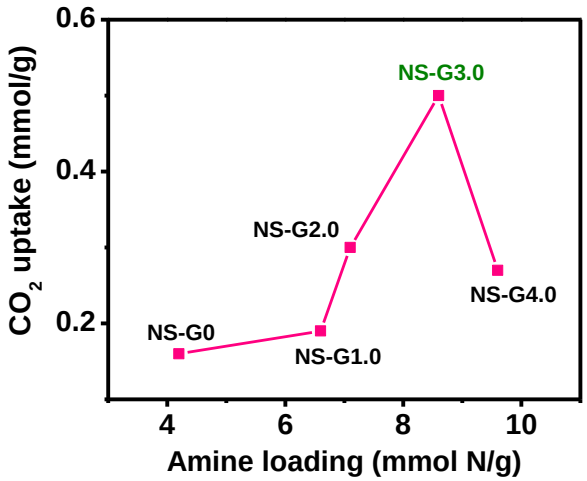

Figure S9. Effect of increasing NS-PAMAM dendrimers on the CO_2 uptake performance.

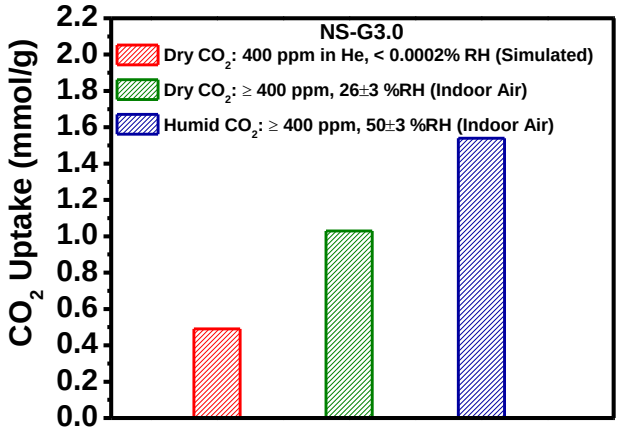

Figure S10. CO_2 uptake (400 ppm CO_2 in He), (≥400 ppm CO_2 in indoor air, 26±3 % RH), and (≥400 ppm CO_2 in indoor air, 50±3 % RH) at 30 °C of NS-G3.0.

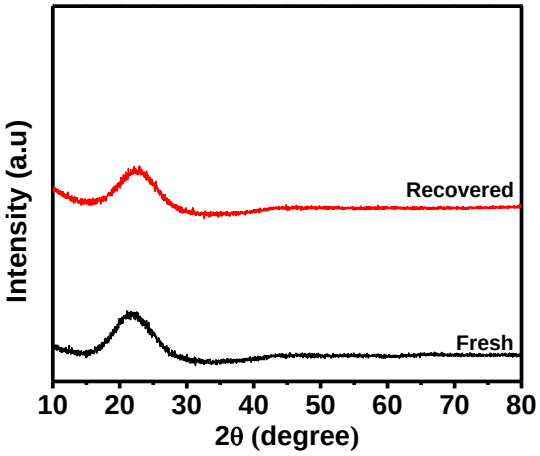

Figure S11. P-XRD studies of NS-G3.0 after 10 successive adsorption-desorption cycles under indoor air (≥400 ppm CO_2, 50±3% RH at 30 °C).

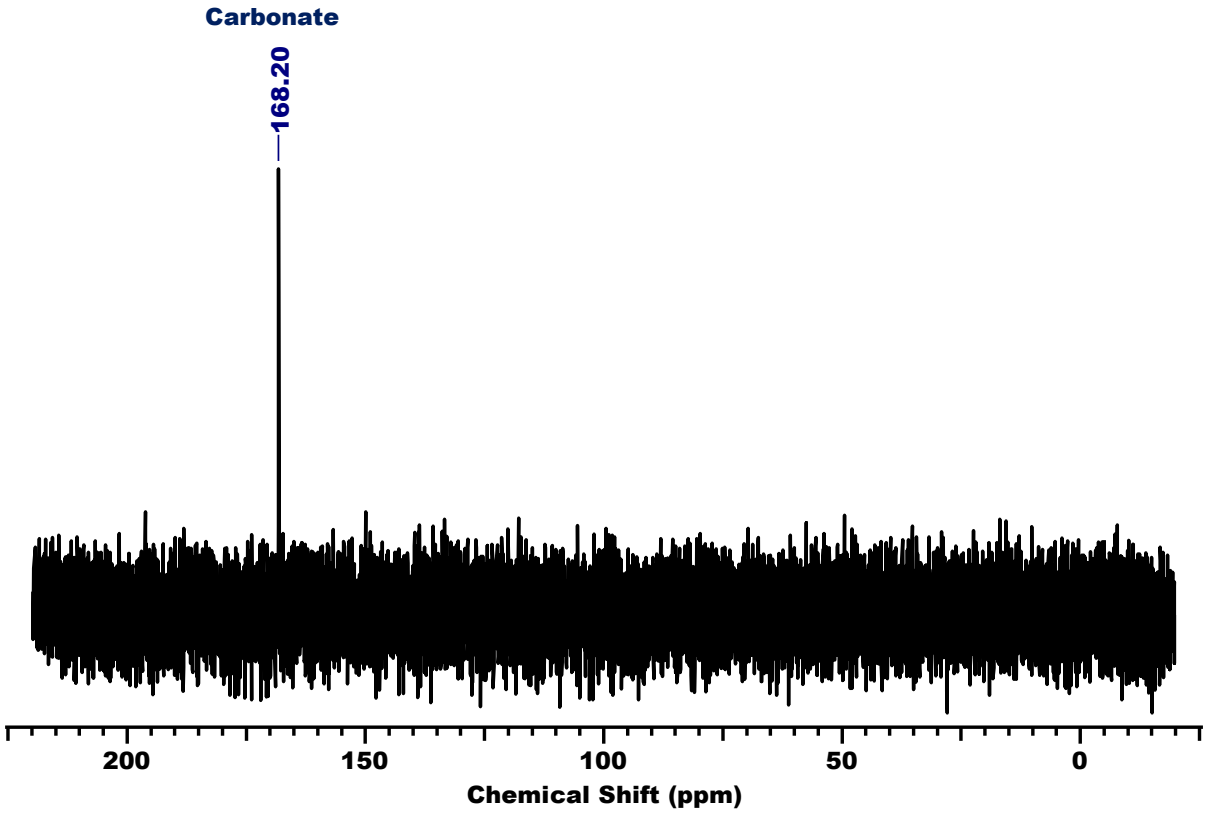

Figure S12. ^{13}C NMR obtained for CO_2 desorption (desorption period: N_2, 0.5 h, 80 °C) and further passed into KOH (1 mmol), water (5 mL).

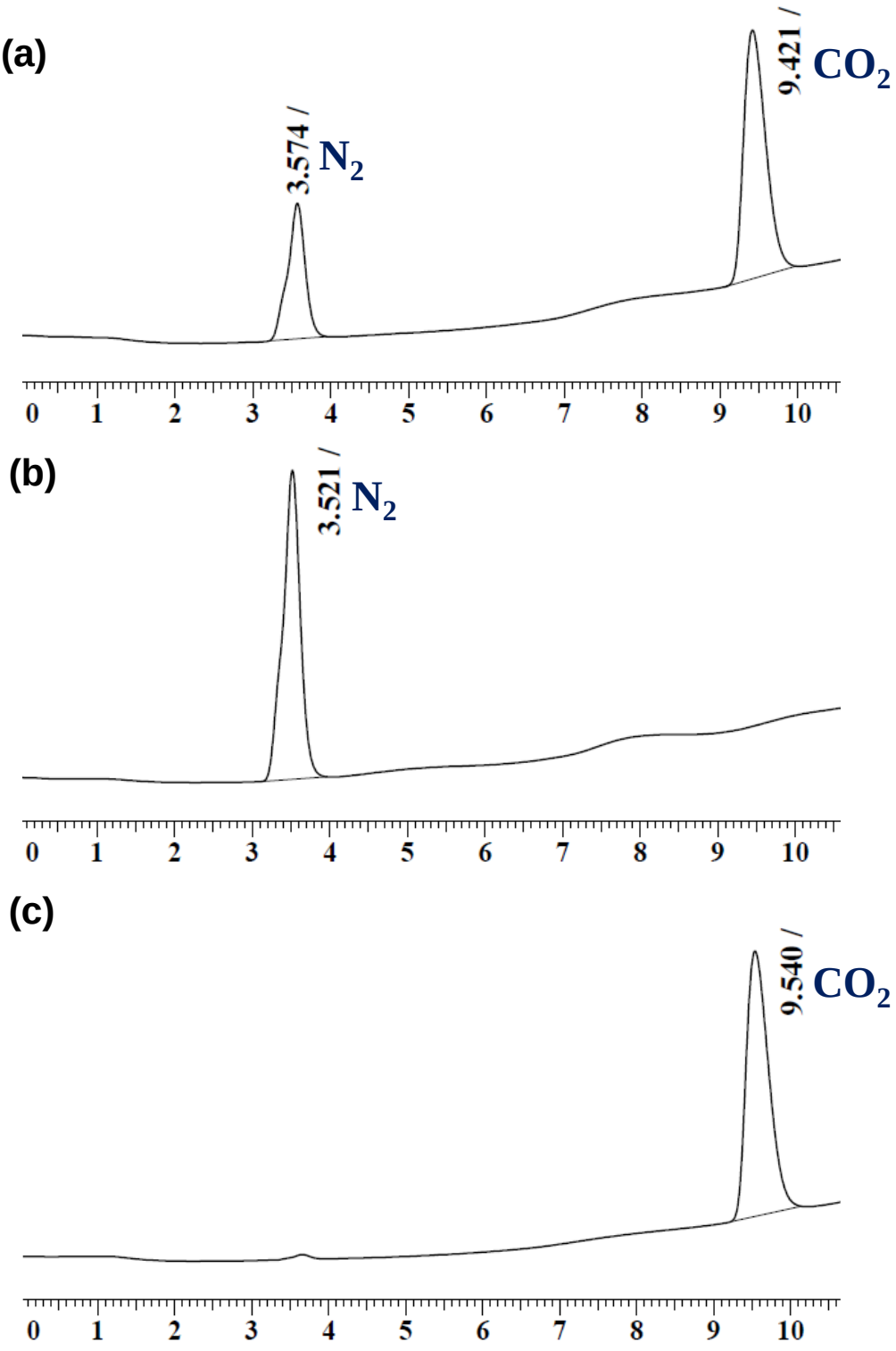

Figure S13. GC-TCD analysis of (a) CO_2 desorbed by NS-G3.0, (b) analysis after CO_2 capture (c) standard pure CO_2 gas (99.999%) (CO_2 adsorption-desorption carried out under ≥400 ppm CO_2, 50 ±3% RH, adsorption period: 0.5 h, 30 °C, and desorption period: N_2, 0.5 h, 80 °C).

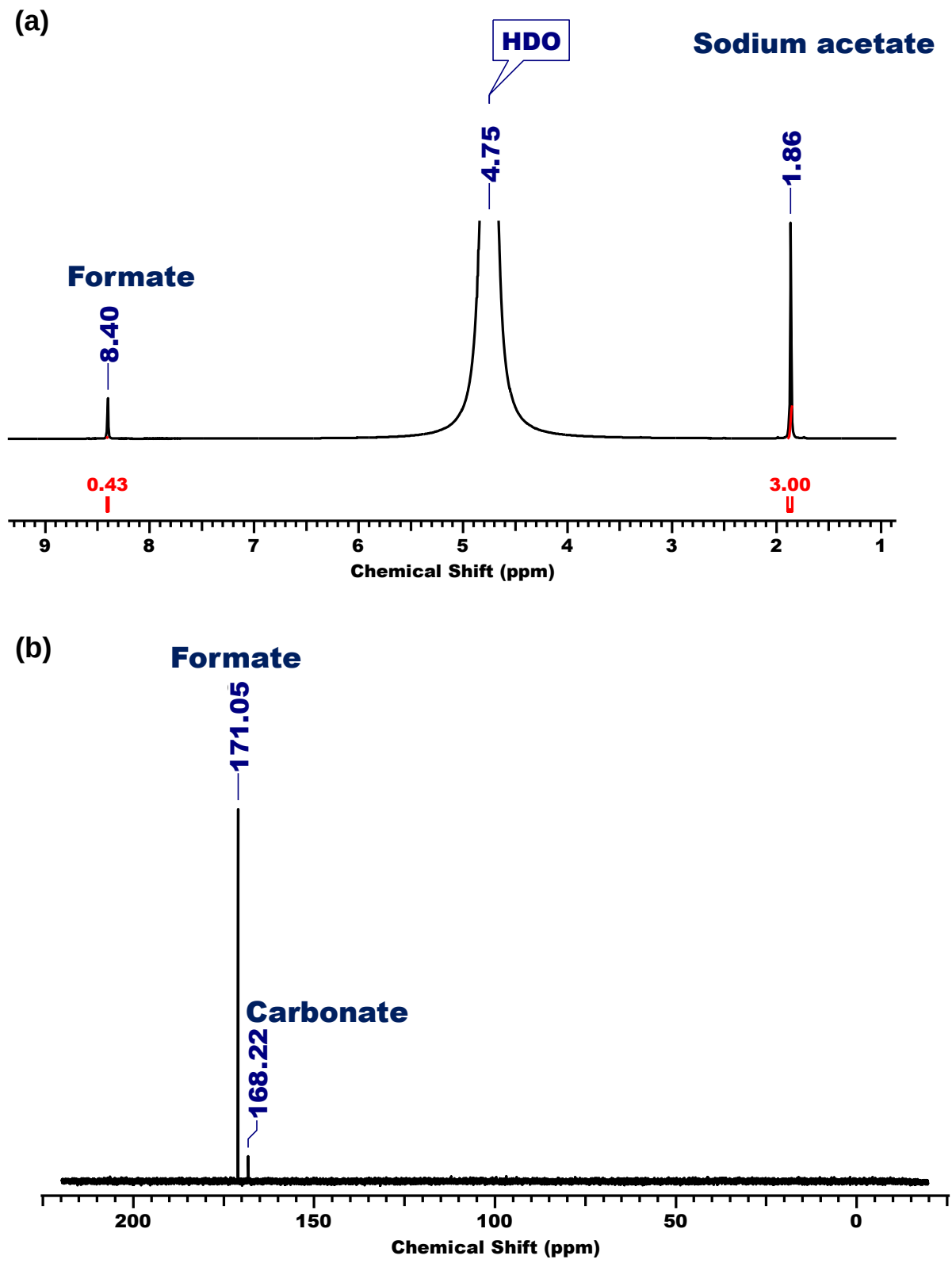

Figure S14. (a) ^{1}H NMR with sodium acetate (0.25 mmol) as the internal standard and (b) ^{13}C NMR spectrum with D_2O as solvent after the hydrogenation of captured CO_2 (CO_3^{2-}) to formate.

General procedure for calculation of formate yield after CO_2/ (bi)carbonate hydrogenation reactions.

For calculating the yield of formate:

$$\mathbf{Y_f} = \frac{\mathbf{I_f \times I_{is} \times V_T}}{\mathbf{V_R}}$$

Where,

Y_f = Yield of formate in mmol

I_f = Integration value of formate

I_{is} = Integration value of internal standard

V_T = Total volume of reaction aliquot (mL)

V_R = Volume of reaction aliquot taken for NMR analysis (mL)

As per the data from Figure S10:

$$\mathbf{Y_f} = \frac{\mathbf{0.43 \times 0.25 \times 5}}{\mathbf{0.54}} = \mathbf{0.99}$$

Table S1 Amine loading[1] on studied adsorbents (from TGA and EDS Analysis).

Material	**N content**	
	From TGA (mmolN/g)	**From EDS analysis (wt%)**
NS	2.7	0.9
NS-G0	4.2	1.2
NS-G0.5	6.2	2.3
NS-G1.0	6.6	2.6
NS-G1.5	6.9	2.7
NS-G2.0	7.1	2.8
NS-G2.5	7.4	3.2
NS-G3.0	8.6	3.4
NS-G3.5	9.2	3.8
NS-G4.0	9.6	4.3

[1]Amine loading is defined as the mass percentage of the amine loss to the total sorbent mass measured from TGA.

Table S2 Textural properties and CO_2 adsorption results of PAMAM dendrimer modified NS.

Material	S_{BET}[a] (m^2/g)	V_{total}[b] (cm^3/g)	Pore diameter (nm)[c]	q_{CO2}[d] (mmol/g) 30 °C, 400 ppm	q_{CO2}[e] (mmol/g) 30 °C, indoor air
NS	912	1.43	3.79	0.09	0.15
NS-G0	178	0.84	3.77	0.16	0.24
NS-G0.5	18	0.09	3.78	0.24	0.43
NS-G1.0	32	0.09	3.77	0.19	0.45
NS-G1.5	23	0.09	3.77	0.23	0.59
NS-G2.0	25	0.09	3.54	0.30	0.61
NS-G2.5	21	0.09	3.43	0.45	1.04
NS-G3.0	**24**	**0.07**	**3.43**	**0.50**	**1.54**
NS-G3.5	20	0.05	3.38	0.28	1.25
NS-G4.0	22	0.02	3.09	0.27	0.84

[a]Specific surface area calculated using BET method (P/P_0 = 0.05-0.30).
[b]Total pore volume calculated from N_2 adsorption at P/P_0 = 0.99.
[c]Pore diameter calculated using NLDFT method.
[d]CO_2 adsorption capacity measured using TGA for 400 ppm CO_2 (simulated air).
[e]CO_2 adsorption capacity measured using TGA for ≥400 ppm CO_2 (indoor air).

Table S3 Comparative chart of CO_2 adsorption performance of amine-based adsorbents under DAC condition.

Support	Amine type	T (°C)	CO_2 conc. (ppm)	Amine loading (mmol N/g)	CO_2 uptake (mmol/g)		Amine efficiency (mmol CO_2/mmol N)	Ref.
					Dry CO_2	Humid CO_2		
Nanosilica	**PAMAM**	**30**	**400**	**8.6**	**0.50**	**-**	**0.06**	**This work**
Nanosilica	**PAMAM**	**30**	**≥400**	**8.6**	**1.02**	**-**	**0.12**	**This work**
Nanosilica	**PAMAM**	**30**	**≥400**	**8.6**	**-**	**1.54[a]**	**0.18**	**This work**
SBA-15	PAMAM	20	90%	-	0.95	-	-	11
SBA-15	PAMAM	30	90%	-	0.45	-	-	12
W-AG-150A	TMPTA	25	400	5.12	0.77	1.09[b]	0.15	13
HBS	TMPTA	25	400	7.73	1.04	-	0.13	14
OHNS	AAMS	25	400	-	0.55		-	15
Mesocellular silica foam	APTMS	25	400	2.70	0.54	-	0.20	16
Mesocellular silica foam	MAPS	25	400	2.41	0.17	-	0.07	16

O-Al_2O_3	APS	30	400	5.43	0.76	-	0.14	[17]
D-Al_2O_3	APS	30	400	4.13	0.62	-	0.15	[17]
Silica gel	AEATPMS	25	400-440	2.48	0.40	0.44[c]	0.16 0.18	[18]
Nano fibrillated Cellulose	AEAPDMS	25	506	4.9	-	1.39[c]	0.28	[19]
Nano fibrillated Cellulose	APDES	23	400	4.9	1.11	2.13[d]	0.26 0.51	[20]
PPN- 6	DETA	22	400	8.5	1.04		0.12	[21]
RFAS	APS	25	400	8.07		1.69[e]	0.21	[22]
SBA-15	APTMS	25	400	-	0.14	0.14[f]	-	[23]
SBA-15 pellet	APTMS	25	400	-	0.09	0.13[f]	-	[23]
SBA- 15	Alkyl halide+ Ammonia	30	400	1.62	0.07	-	0.043	[24]
Pore-expanded MCM-41	TMPTA	30	400	7.9	0.64	0.55[h]	-	[25]
Pore-expanded MCM-41	TMPTA	25	400	7.9	0.98	-	0.12	[26]
Mg_2(dobpdc)	Ethylenediamine	25	390	-	2.83	-	-	[27]
Mg_2(dobdc)	Hydrazine	25	400	6.01	3.89	-	-	[28]
Mg-MOF-74	Ethylenediamine	25	400		1.51	-	-	[29]
Mg_2(dobpdc)	mmen	25	390	-	2.0	-	-	[30]
Cr-MIL-101-SO_3H	TAEA	20	400		1.12	-	-	[31]
SBA- 15	Z-l-Lysine+ APTMS	25	400	5.18	0.60	-	0.12	[32]
Hybrid silica	APS	30	400	4.5	-	1.68[i]	0.37	[33]
SBA- 15	Aziridine	25	400	9.9	-	1.72[j]	0.17	[34]
AHTSA	APS	30	400	8.47	1.64	-	0.19	[35]
Macroporous Silica	L-alanine	50	400	10.98	2.65	-	0.24	[36]

[a] 50±3% humidity; [b] 53% humidity; [c] 40% humidity; [d] 91% relative humidity; [e] 4% relative humidity; [f] 80% relative humidity; [g] 49% relative humidity; [h] 73% relative humidity; [i] 60% relative humidity; [j]fully humified condition; APS: (3-aminopropyl) triethoxysilane; TMPTA: N^1-(3-trimethoxysilylpropyl)diethylenetriamine; AAMS: N-(2-aminoethyl)-3-aminopropylmethyldiethoxysilane; APTMS: (3-aminopropyl) trimethoxysilane; MAPS: N-methylaminopropyl trimethoxysilane; AEATPMS: N-(3-(trimethoxysilyl) propyl) ethane-1,2-diamine, AEAPDMS: N-2-aminoethyl-3-aminopropylmethyldimethoxysilane; APDES: 3-Aminopropyl-methyl-diethoxysilane; DETA: diethylenetriamine; mmen, N,N′-

dimethylethylenediamine; TAEA: tris(2-aminoethyl)amine. TRI, 2-[2-(3-trimethoxysilylpropylamino)ethylamino]ethylamine, AHTSA, amine hybrid titania/silsesquioxane composite aerogel.

Table S4 Comparative chart of amine-based sorbent regeneration and cyclic CO_2 adsorption-desorption stability for DAC applications.

Support	**Amine type**	**Sorbent regeneration condition**	**Stability performance**	**Ref.**
Nano Silica	**PAMAM**	**80 °C for 0.5 h under vacuum**	**No capacity loss over 10 cyclic runs**	**This work**
Hierarchical Silica	APS	110 °C for 0.5 h under N_2 flow at 20 mL/min	13% capacity loss in 5 cyclic runs	[37]
Hierarchical Silica	TMPTA	110 °C for 0.5 h under N_2 flow at 20 mL/min	15% capacity loss in 5 cyclic runs	[37]
Pore-expanded MCM-41	TMPTA	100 °C for 15 min by synthetic air at 10 mL/min	~24% capacity loss in 4 cyclic runs[1]	[25]
Silica	PEI	110 °C for 3 h under Ar flow at 100 mL/min	30.1% capacity loss in 4 cyclic runs	[38]
Silica	A-PEI	110 °C for 3 h under Ar flow at 100 mL/min	9.3% capacity loss in 4 cyclic runs	[38]
Silica	T-PEI	110 °C for 3 h under Ar flow at 100 mL/min	1.36% capacity loss in 4 cyclic runs	[38]
Fumed Silica	PEI	85 °C for 3 h under vacuum	3.5% capacity loss in 4 cyclic runs	[39]
Hierarchical Silica	PEI	110 °C for 6 h under He flow at 100 mL/min	16% capacity loss in 5 cyclic runs humid condition, whereas no appreciable change in CO_2 adsorption capacity in dry condition	[40]
SBA-15	PEI	110 °C for 9 h under Ar flow at 100 mL/min	Stable over short multicycle operations (3 cyclic runs)	[41]

CA-SiO_2	PEI	110 °C for 2 h under He flow	9.6% pseudo-equilibrium capacity and 16% breakthrough capacity loss in 20 cyclic runs	[8]
Mg_2(dobpdc)	en	150 °C for 2 h under simulated air (0.39 mbar CO_2) purge at 60 mL/min	6% capacity loss in 5 cyclic runs	[27]
MIL-101-Cr	PEI	110 °C for 3 h under He flow at 90 mL/min	CO_2 uptake dropped 2.7 % and 1.9% after the first and second cycles, respectively (total 3 cyclic runs)	[42]

[1]Data retrieved from Data from graph software (Version 1.0) APS/APTES: 3-(aminopropyl)triethoxysilane ;TMPTA: 2-[2-(3-trimethoxysilylpropylamino) ethylamino]ethylamine; TEPA: tetraethylenepentamine; PEI: polyethyleneimine; A-PEI: 3-(aminopropyl)triethoxysilane-PEI, T-PEI: tetrapropyl orthotitanate-PEI, en: ethylenediamine)

References:

1 C. A. R. Costa, C. A. P. Leite and F. Galembeck, *J. Phys. Chem. B*, 2003, **107**, 4747–4755.

2 X. Du and J. He, *Nanoscale*, 2012, **4**, 852–859.

3 R. J. Kalbasi and F. Zamani, *RSC Adv.*, 2014, **4**, 7444–7453.

4 A. A. Al-Absi, M. Mohamedali, A. Domin, A. M. Benneker and N. Mahinpey, *Chem. Eng. J.*, 2022, **447**, 137465.

5 G. Calleja, R. Sanz, A. Arencibia and E. S. Sanz-Pérez, in *Topics in Catalysis*, Springer, 2011, **54**, 135–145.

6 B. Ferreira dos Santos, J. A. Cecilia, M. Bastos-Neto, E. Rodríguez-Castellón, D. C. Silva de Azevedo and E. Vilarrasa-García, *Chem. Eng. Res. Des.*, 2022, **177**, 583–593.

7 A. Gutierrez-Ortega, R. Nomen, J. Sempere, J. B. Parra, M. A. Montes-Morán and R. Gonzalez-Olmos, *Chem. Eng. J.*, 2022, **435**, 134703.

8 A. R. Sujan, S. H. Pang, G. Zhu, C. W. Jones and R. P. Lively, *ACS Sustain. Chem. Eng.*, 2019, **7**, 5264–5273.

9 D. R. Kumar, C. Rosu, A. R. Sujan, M. A. Sakwa-Novak, E. W. Ping and C. W. Jones, *ACS Sustain. Chem. Eng.*, 2020, **8**, 10971–10982.

10 S. J. Han, M. Yoo, D. W. Kim and J. H. Wee, *Energy Fuels*, 2011, **25**, 3825–3834.

11 Z. Liang, B. Fadhel, C. J. Schneider and A. L. Chaffee, *Microporous Mesoporous Mater.*, 2008, **111**, 536–543.

12 Y. Jing, L. Wei, Y. Wang and Y. Yu, *Microporous Mesoporous Mater.*, 2014, **183**, 124–133.

13 J. T. Anyanwu, Y. Wang and R. T. Yang, *Ind. Eng. Chem. Res.*, 2020, **59**, 7072–7079.

14 J. T. Anyanwu, Y. Wang and R. T. Yang, *Chem. Eng. J.*, 2022, **427**, 131561.

15 K. Suresh, K. Reddy, A. M. Varghese, A. E. Ogungbenro and G. N. Karanikolos, 2023,

2, 720–733.

16 S. A. Didas, A. R. Kulkarni, D. S. Sholl and C. W. Jones, *ChemSusChem*, 2012, **5**, 2058–2064.

17 M. E. Potter, K. M. Cho, J. J. Lee and C. W. Jones, *ChemSusChem*, 2017, **10**, 2192–2201.

18 J. A. Wurzbacher, C. Gebald and A. Steinfeld, *Energy Environ. Sci.*, 2011, **4**, 3584–3592.

19 C. Gebald, J. A. Wurzbacher, P. Tingaut, T. Zimmermann and A. Steinfeld, *Environ. Sci. Technol.*, 2011, **45**, 9101–9108.

20 C. Gebald, J. A. Wurzbacher, A. Borgschulte, T. Zimmermann and A. Steinfeld, *Environ. Sci. Technol.*, 2014, **48**, 2497–2504.

21 W. Lu, J. P. Sculley, D. Yuan, R. Krishna and H. C. Zhou, *J. Phys. Chem. C*, 2013, **117**, 4057–4061.

22 L. He, M. Fan, B. Dutcher, S. Cui, X. dong Shen, Y. Kong, A. G. Russell and P. McCurdy, *Chem. Eng. J.*, 2012, **189**–**190**, 13–23.

23 N. R. Stuckert and R. T. Yang, *Environ. Sci. Technol.*, 2011, **45**, 10257–10264.

24 E. G. Moschetta, M. A. Sakwa-Novak, J. L. Greenfield and C. W. Jones, *Langmuir*, 2015, **31**, 2218–2227.

25 A. Wagner, B. Steen, G. Johansson, E. Zanghellini, P. Jacobsson and P. Johansson, *Int. J. Spectrosc.*, 2013, **2013**, 1–8.

26 Y. Belmabkhout, R. Serna-Guerrero and A. Sayari, *Ind. Eng. Chem. Res.*, 2010, **49**, 359–365.

27 W. R. Lee, S. Y. Hwang, D. W. Ryu, K. S. Lim, S. S. Han, D. Moon, J. Choi and C. S. Hong, *Energy Environ. Sci.*, 2014, **7**, 744–751.

28 P. Q. Liao, X. W. Chen, S. Y. Liu, X. Y. Li, Y. T. Xu, M. Tang, Z. Rui, H. Ji, J. P. Zhang and X. M. Chen, *Chem. Sci.*, 2016, **7**, 6528–6533.

29 S. Choi, T. Watanabe, T. H. Bae, D. S. Sholl and C. W. Jones, *J. Phys. Chem. Lett.*, 2012, **3**, 1136–1141.

30 T. M. McDonald, W. R. Lee, J. A. Mason, B. M. Wiers, C. S. Hong and J. R. Long, *J. Am. Chem. Soc.*, 2012, **134**, 7056–7065.

31 H. Li, K. Wang, D. Feng, Y. P. Chen, W. Verdegaal and H. C. Zhou, *ChemSusChem*, 2016, **9**, 2832–2840.

32 W. Chaikittisilp, J. D. Lunn, D. F. Shantz and C. W. Jones, *Chem. – A Eur. J.*, 2011, **17**, 10556–10561.

33 K. A. S. Abhilash, T. Deepthi, R. A. Sadhana and K. G. Benny, *ACS Appl. Mater. Interfaces*, 2015, **7**, 17969–17976.

34 S. Choi, J. H. Drese, P. M. Eisenberger and C. W. Jones, *Environ. Sci. Technol.*, 2011, **45**, 2420–2427.

35 Y. Kong, G. Jiang, Y. Wu, S. Cui and X. Shen, *Chem. Eng. J.*, 2016, **306**, 362–368.

36 F. Q. Liu, L. Wang, Z. G. Huang, C. Q. Li, W. Li, R. X. Li and W. H. Li, *ACS Appl. Mater. Interfaces*, 2014, **6**, 4371–4381.

37 V. Kulkarni, J. Parthiban and S. K. Singh, *Microporous Mesoporous Mater.*, 2024, **368**, 112998.

38 S. Choi, M. L. Gray and C. W. Jones, *ChemSusChem*, 2011, **4**, 628–635.

39 A. Goeppert, M. Czaun, R. B. May, G. K. S. Prakash, G. A. Olah and S. R. Narayanan, *J. Am. Chem. Soc.*, 2011, **133**, 20164–20167.

40 H. T. Kwon, M. A. Sakwa-Novak, S. H. Pang, A. R. Sujan, E. W. Ping and C. W. Jones, *Chem. Mater.*, 2019, **31**, 5229–5237.

41 W. Chaikittisilp, H. J. Kim and C. W. Jones, *Energy and Fuels*, 2011, **25**, 5528–5537.

42 L. A. Darunte, A. D. Oetomo, K. S. Walton, D. S. Sholl and C. W. Jones, *ACS Sustain. Chem. Eng.*, 2016, **4**, 5761–5768.